# Thermal structure of a gas-permeable lava dome and timescale separation in its response to perturbation

Peter D. Hicks,[1] Adrian J. Matthews,[1,2] and Mark J. Cooker[1]

[1] The thermal boundary layer at the surface of a volcanic lava dome is investigated through a continuum model of the thermodynamic advection-diffusion processes resulting from magmatic gas flow through the dome matrix. The magmatic gas mass flux, porosity, and permeability of the rock are identified as key parameters. New, theoretical, nonlinear steady state thermal profiles are reported, which give a realistic surface temperature of 210°C for a region of lava dome surface through which a gas flux of $3.5 \times 10^{-3}$ kg s$^{-1}$ m$^{-2}$ passes. This contrasts favorably with earlier purely diffusive thermal models, which cool too quickly. Results are presented for time-dependent perturbations of the steady states as a response to changes in surface pressure, a sudden rockfall from the lava dome surface, and a change in the magmatic gas mass flux at depth. Together with a generalized analysis using the method of multiple scales, this identifies two characteristic timescales associated with the thermal evolution of a dome carapace: a short timescale of several minutes, over which the magmatic gas mass flux, density, and pressure change to a new quasi-steady state and a longer timescale of several days, over which the thermal profile changes to a new equilibrium distribution. Over the longer timescale, the dynamic properties of the dome continue to evolve, but only in slavish response to the ongoing temperature evolution. In light of this timescale separation, the use of surface temperature measurements to infer changes in the magmatic gas flux for use in volcanic hazard prediction is discussed.

Citation: Hicks, P. D., A. J. Matthews, and M. J. Cooker (2009), Thermal structure of a gas-permeable lava dome and timescale separation in its response to perturbation, *J. Geophys. Res.*, *114*, B07201, doi:10.1029/2008JB006198.

## 1. Introduction

[2] Lava domes are steep-sided, mounds of lava, formed by extrusion of highly viscous lava from volcanic vents. Their rheology is due to the high silica content of the source magma; typically dacitic, rhyolitic, or andesitic volcanoes located in subduction settings. There are two main styles of lava dome growth: endogenous and exogenous. An endogenous dome forms by internal emplacement of magma at the base of the dome from the magma conduit below. It has a layered internal structure. In exogenous dome growth, fresh magma forces its way to the surface, leading to surface features such as spines and lobes. Dome growth can switch between these two styles on the same volcano, e.g., at Unzen [*Nakada et al.*, 1995] and Soufrière Hills Volcano [*Watts et al.*, 2002].

[3] As magma ascends in the conduit, its depressurization leads to the exsolution of dissolved volatiles and the production of magmatic gas. These gases form bubbles, and lead to degassing-induced crystallization and an increase in viscosity [*Sparks*, 1997]. The bubbles can also form interconnected pathways through the lava, making it permeable to gas flow. An internal gas pressure gradient drives the gas upward through the conduit and the dome above, which then escapes into the atmosphere. Heat advection by this gas provides an important mechanism of heat transfer within a dome, in addition to diffusion.

[4] Lava domes have several associated hazards. Under certain circumstances, the high internal pressures can lead to failure, resulting in explosions, dome collapse and pyroclastic flows [*Fink and Kieffer*, 1993; *Calder et al.*, 2002]. The overpressures that lead to these failures can be triggered by sudden increases in magmatic gas flux [*Sparks*, 1997]. Collapse can also be triggered by gravitational instability if a dome outgrows the confines of the volcano summit and if it cannot be supported by the flanking talus slopes [*Sato et al.*, 1992]. External triggers can also lead to hazardous volcanic activity [*Neuberg*, 2000]. In particular, intense rainfall has been shown to initiate explosions, dome collapses and pyroclastic flows [*Mastin*, 1994; *Yamasato et al.*, 1998; *Matthews et al.*, 2002; *Carn et al.*, 2004; *Barclay et al.*, 2006]. Hence an understanding of the internal structure of a dome and the conditions that can lead to failure are important from a natural hazards perspective.

[5] Due to the hostile conditions around active lava domes, basic physical parameters are difficult to measure.

[1] School of Mathematics, University of East Anglia, Norwich, UK.
[2] School of Environmental Sciences, University of East Anglia, Norwich, UK.

Blackbody surface temperatures of around $200-350°C$ have been inferred from measurements of the infrared radiation emitted from a dome surface [*Dzurisin et al.*, 1990; *Oppenheimer et al.*, 1993; *Urai*, 2000]. Surface rockfalls expose hotter rock immediately below. Similarly observations of incandescence, lead to estimated temperatures near $650°C$ at a depth of approximately one metro [*Sparks et al.*, 2000; *Watts et al.*, 2002]. The temperature increases further with depth within a surface carapace layer, with a typical thickness of $10-30$ m [*Iverson*, 1990]. Below this, the temperature is expected to be isothermal from theoretical considerations [*Melnik and Sparks*, 1999] with a value near $830°C$ [*Barclay et al.*, 1998].

[6] The total volume of a dome can be measured by photogrammetric-GPS techniques, and the growth rate inferred [*Herd et al.*, 2005]. The composition and mass flux of magmatic gases emitted from the dome surface can be detected by remote spectroscopic techniques [*Francis et al.*, 2000; *Edmonds et al.*, 2001]. Additionally, chemical composition and bulk physical properties of field specimens of dome rock can be measured in the laboratory. These include density, specific heat capacity, thermal conductivity, porosity and permeability [*Sigurdsson*, 2000; *Spera*, 2000; *Couch et al.*, 2001]. In summary, many key parameters of volcanic domes are known incompletely, and with large error bounds. Several of these parameters, such as surface temperature and magmatic gas flux, also exhibit considerable natural variability, both temporally and spatially over a dome.

[7] Models of dome growth and evolution should predict parameter values that fall within the range of these observations. For example, in a one-dimensional model of the flow of magmatic gas through a lava dome, *Woods et al.* [2002] calculated the steady state profiles of gas pressure as a function of depth within a permeable dome. *Woods et al.* [2002] predict realistic pressure profiles within a dome, below the carapace region. However, their model was assumed to be isothermal and neglected the role of the thermal boundary layer upon the pressure profile. One-dimensional models of the thermal structure of an impermeable lava dome have been considered by *Matthews and Barclay* [2004]. As there was no advection of heat by magmatic gases, the only mechanism for vertical heat flow in the interior was diffusion. This led to unrealistically rapid cooling and low surface temperatures.

[8] Several models of lava dome growth have also been proposed, employing either asymptotic studies exploiting the typical small aspect ratio of dome height to horizontal extent [*Balmforth et al.*, 2000, 2004; *Dragoni et al.*, 2005] or numerical simulations using the finite element level set method [*Hale and Wadge*, 2003; *Bourgouin et al.*, 2007; *Hale et al.*, 2007]. These models were successful in generating realistic dome geometries and free surface evolution for endogenous growth. However, these models were either isothermal or, in cases where temperature was allowed to vary, the only heat transfer mechanism was thermal diffusion in the dome matrix. As a consequence, they did not simulate realistic thermal profiles. Again, this is likely to be due to the assumption of an impermeable dome and the omission of a magmatic gas flux and its associated heat advection.

[9] In this paper, we build on previous modeling studies of energy fluxes through a volcanic dome. We develop a model that includes both the diffusion of heat in the dome carapace, and the advection of heat by magmatic gas flow through the surface carapace layer of a permeable dome. Together with a parameterization of energy fluxes at the dome surface, the model then generates steady state surface temperatures, and temperature and pressure profiles within a dome, in good agreement with observations. For example, in a region of the lava dome surface through which a gas mass flux of $3.5 \times 10^{-3}$ kg s$^{-1}$ m$^{-2}$ passes, the predicted steady state surface temperature is $210°C$. To investigate the stability of a dome to external forcing, the steady state temperature and pressure solutions can then be subjected to a range of time-dependent perturbations. These could include:

[10] 1. a change in surface pressure due to the passage of a weather system;

[11] 2. removal of surface material due to rockfall;

[12] 3. a change in the flux of magmatic gas at depth;

[13] 4. the impact of rainfall on the surface of a dome.

[14] Perturbations $1-3$ will be examined during the course of this paper, and their implications for lava dome failure discussed. For each perturbation, the time-dependent evolution of the lava dome temperature, and the magmatic gas pressure, density and volume flux profiles will be investigated. The model reveals a characteristic timescale separation between the thermal response of the lava dome and the dynamic response of the magmatic gas. This is investigated further using the technique of multiple-scale analysis. Perturbations to volcanic domes by rainfall (number 4 in the list above) have been shown in previous modeling studies to lead to instability and failure [*Matthews and Barclay*, 2004; *Elsworth et al.*, 2004; *Simmons et al.*, 2004; *Taron et al.*, 2007]. The response to rainfall of the volcanic dome model developed here will form the basis of a subsequent paper.

## 2. Development of a Model for a Gas-Permeable Lava Dome

[15] In this section, we develop a thermodynamic model of the temperature evolution of a lava dome carapace, combined with the magmatic gas flow.

### 2.1. Assumptions

[16] We consider an idealized lava dome consisting of a porous rock matrix (hereafter referred to as "matrix") whose physical properties correspond to those of a typical andesite. The void spaces, which incorporate both the effects of cracks and vesicles are assumed to be isotropically distributed. The porous medium is assumed to be rigid, while magmatic gas is forced upward through the connected void spaces.

[17] Two key properties in any model for porous media flow are the porosity (the proportion of the lava dome which is not occupied by andesite) and the permeability of the andesite which is a measure of the ease of gas flow through the pore spaces and fracture network. [*Melnik and Sparks*, 2002] report laboratory measurements of porosity and permeability for a range of andesite samples from the Soufrière Hills Volcano. These range from a porosity of 0.023 and a permeability of $6 \times 10^{-16}$ m$^2$ for dense "glassy" fragments to a porosity of 0.72 porous and a permeability of $4 \times 10^{-12}$ m$^2$ for pumice. In the absence of

**Table 1.** Typical Physical Properties of Andesite Used in the Model

|  | Property | Value |
|---|---|---|
| $k_r$ | thermal conductivity | 2.6 W m$^{-1}$ K$^{-1}$ |
| $c_r$ | specific heat capacity | 1000 J kg$^{-1}$ K$^{-1}$ |
| $\rho_r$ | density | 2600 kg m$^{-3}$ |
| $\phi$ | porosity | 0.2 |
| $\mathcal{K}$ | permeability | $10^{-11}$ m$^2$ |

detailed information regarding the composition and structure of the dome it is difficult to estimate bulk properties from these measurements. The range of permissible permeability values used in our investigations is further limited by the requirement that the magmastatic gas pressure cannot dramatically exceed the magmastatic overburden pressure for extended periods of time. *Costa* [2006] fitted the classical Kozeny-Carman relationship it these samples and in general the complicated lava dome evolution will produce large spatial inhomogeneities in both porosity and permeability. However, for simplicity and following the earlier work of *Woods et al.* [2002], we shall assume homogeneous distributions of porosity and permeability. These can be interpreted as either global averages over the whole dome or localized representations of the features and regions making up the dome. The values of the physical properties of andesite are given in Table 1.

[18] The matrix and the magmatic gas passing through the void spaces are assumed to be in local thermal equilibrium, which means that at any point they share one common temperature. This allows the conservation of energy within both the matrix and the magmatic gas to be written as a single equation. Energy is transferred through the solid carapace of the lava dome by a combination of diffusion in the matrix and magmatic gas, and advection of the magmatic gas. The composition of a sample of magmatic gas from the Soufrière Hills Volcano was shown to be in excess of 90% water by volume [*Hammouya et al.*, 1998]. For simplicity, we assume that the thermal conductivity, specific heat capacity and viscosity of the magmatic gas take the same values as the equivalent properties of water vapor. The values of these physical properties are given in Table 2.

[19] Typical dome structures are approximately isothermal below a surface carapace region of approximately 30 m thickness [*Iverson*, 1990]. In the model developed the temperature at the base of the carapace region is maintained at 1100 K (the temperature of fresh magma extrusion from the conduit [*Barclay et al.*, 1998]), but the behavior of the model is insensitive to the position of this interface.

[20] The total magmatic gas flux can be estimated from measurements of the sulfur dioxide ($SO_2$) gas flux. This is highly variable on many timescales. Typical values at the Soufrière Hills Volcano lie in the range 0.1–50 kg s$^{-1}$ [*Edmonds et al.*, 2003a, 2003b]. The mixing ratio of $SO_2$ in magmatic gas is approximately 15:1, hence the total magmatic gas flux lies in the range 1.5–750 kg s$^{-1}$. The surface area of the Soufrière Hills Volcano dome is approximately $5 \times 10^5$ m$^2$ [*Carn et al.*, 2004], giving an average mass flux per unit area of up to $1.5 \times 10^{-3}$ kg s$^{-1}$ m$^{-2}$. However, the

emission of magmatic gas is not uniformly distributed over the surface of a dome, with cracks and fissures in the structure of a dome matrix acting to channel above-average magmatic gas fluxes to certain regions of a dome, while large regions of the dome periphery may have little or no magmatic gas passing through them. Our contention is that the flux of heat resulting from the advection of magmatic gas is vital in describing the thermal structure of a dome, and therefore in order to generate lava dome surface temperatures corresponding to the maximum values recorded in the literature, it makes sense to consider the thermal structure of regions of small horizontal extent, but through which a magmatic gas flux, perhaps an order of magnitude above the background average may flow.

## 2.2. Derivation of Model Equations

[21] We consider a system of one-dimensional conservation laws describing the flow of energy, mass, and momentum in the direction along the outward normal to the lava dome surface and at an angle $\alpha$ to gravity. This is the $\tilde{z}$ axis where $\tilde{z} = 0$ is at the dome surface, the atmosphere above the dome is in the region $\tilde{z} > 0$ and the dome itself is in the region $\tilde{z} < 0$. The lower boundary of the model is at $\tilde{z} = -L$ for some positive constant $L$ (as shown in Figure 1). This system connects the behavior of the solid dome matrix phase (whose properties are represented by a subscript $r$ for "rock") to the properties of the magmatic gas (whose properties are represented by subscript $g$ for "gas").

[22] In the model equations variables with a tilde ($\sim$) are dimensional quantities, variables with a caret ($\wedge$) are nondimensional quantities and symbols with neither a tilde nor a caret are dimensional, physical constants. The porosity ($\phi$) and density ($\rho_r$) of the matrix are assumed to be constant, while the density ($\tilde{\rho}_g$) and volume flux per unit cross-sectional area of void space, or equivalently the average flow speed of magmatic gas ($\tilde{v}_g$) vary. Under these assumptions, conservation of energy allows us to write an equation governing the combined rock matrix and magmatic gas temperature $\tilde{T}$, itself a function of the level $\tilde{z}$ and time $\tilde{t}$, in the form

$$\frac{\partial}{\partial \tilde{t}}\left[\left\{(1-\phi)c_r\rho_r + \phi c_g\tilde{\rho}_g\right\}\tilde{T}\right]$$
$$+ \frac{\partial}{\partial \tilde{z}}\left(\phi c_g\tilde{\rho}_g\tilde{v}_g\tilde{T}\right) - \frac{\partial}{\partial \tilde{z}}\left(k_e\frac{\partial \tilde{T}}{\partial \tilde{z}}\right) = 0, \qquad (1)$$

where the specific heat capacities of the matrix and magmatic gases are $c_r$ and $c_g$, respectively. The effective thermal conductivity $k_e$, is assumed to satisfy the parallel model $k_e = (1-\phi)k_r + \phi k_g$, with $k_r$ and $k_g$ being the thermal conductivities of the andesite and magmatic gas phases, respectively. The effective thermal conductivity allows us to combine the thermal diffusion in andesite and magmatic gas

**Table 2.** Typical Physical Properties of Magmatic Gas Used in the Model (Based on Physical Properties of Water Vapor)

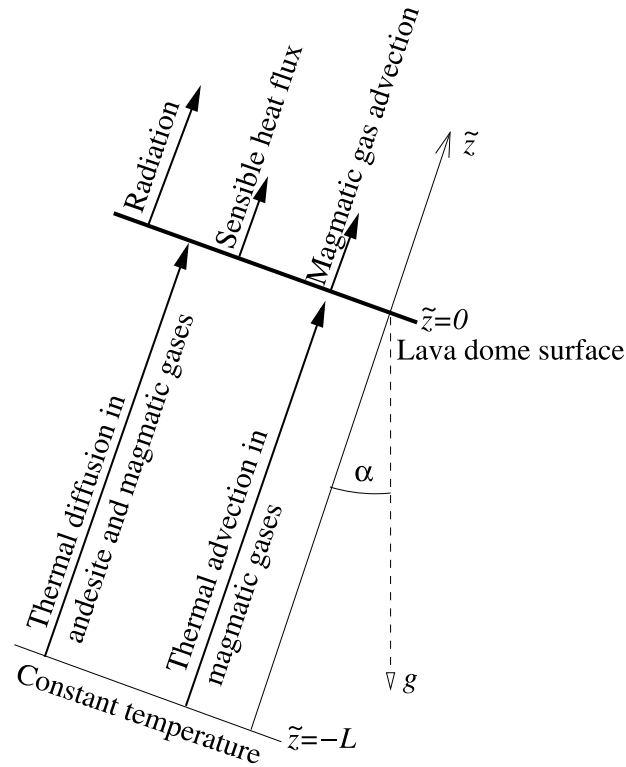|  | Property | Value |
|---|---|---|
| $k_g$ | thermal conductivity | 0.016 W m$^{-1}$ K$^{-1}$ |
| $c_g$ | specific heat capacity | 2026 J kg$^{-1}$ K$^{-1}$ |
| $\mu_g$ | viscosity | $2.82 \times 10^{-4}$ Pa s |

**Figure 1.** Schematic diagram showing diffusive heat fluxes in the dome matrix and magmatic gas and advective heat fluxes in the magmatic gas in a dome interior. Surface heat fluxes are due to radiation, atmospheric convection, and magmatic gas advection. All heat fluxes are assumed to be perpendicular to the lava dome surface and at an angle $\alpha$ to the vertical direction.

into one term. For an isotropic porosity distribution and constant thermal conductivities, the effective thermal conductivity and the first derivative of the final term in equation (1) can be interchanged. The second term in equation (1) corresponds to thermal advection in the magmatic gas.

[23] Mass conservation of magmatic gas rising up through the permeable matrix is governed by

$$\phi \frac{\partial \tilde{\rho}_g}{\partial \tilde{t}} + \phi \frac{\partial}{\partial \tilde{z}}\left(\tilde{\rho}_g \tilde{v}_g\right) = 0. \qquad (2)$$

Conservation of momentum for the magmatic gas occupying the void spaces of the porous medium is assumed to be given by Darcy's law which relates the volume flux to the pressure gradient in the magmatic gas. If the total pressure in the magmatic gas is $\tilde{p}_g$, then

$$\tilde{v}_g = -\frac{\mathcal{K}}{\phi \mu_g}\left(\frac{\partial \tilde{p}_g}{\partial \tilde{z}} + \tilde{\rho}_g g \cos \alpha\right), \qquad (3)$$

where the constant of proportionality between the volume flux and pressure gradient includes the andesite perme-

ability $\mathcal{K}$, the porosity $\phi$, and the viscosity $\mu_g$ of the magmatic gas. The second term on the right-hand side of equation (3) is the correction due to gravity with $g$ representing the acceleration due to gravity and $\alpha$ the angle between the vertical and the normal to the lava dome surface (Figure 1). This system of governing equations becomes closed with an equation of state for the magmatic gas. Magmatic gas is assumed to behave like an ideal gas and is governed by

$$\tilde{p}_g = \tilde{\rho}_g \mathcal{R}_g \tilde{T}, \qquad (4)$$

where $\mathcal{R}_g = 461.5$ J kg$^{-1}$ K$^{-1}$ is the ideal gas constant for water vapor.

### 2.3. Boundary Conditions

[24] To complete this system of equations, we need boundary conditions at the surface ($\tilde{z} = 0$) and at some fixed level ($\tilde{z} = -L$) inside the lava dome. At the dome surface the difference between the surface temperature $\tilde{T}_s(t) = \tilde{T}(\tilde{z} = 0, t)$ and the temperature of the atmosphere $T_a$ generates a flux of heat away from the volcano which is a combination of radiative and convective (sensible) components [*Neri*, 1998; *Carn et al.*, 2004]

$$-k_e \frac{\partial \tilde{T}}{\partial \tilde{z}}\bigg|_{\tilde{z}=0} = \epsilon_s \sigma\left(\tilde{T}_s^4 - T_a^4\right) + S_h \rho_a c_a U\left(\tilde{T}_s - T_a\right), \qquad (5)$$

where in the radiative heat flux term $\epsilon_s = 0.95$ is the emissivity of the andesite, $\sigma = 5.67 \times 10^{-8}$ W m$^{-2}$ K$^{-4}$ is the Stefan-Boltzmann constant and in the convective heat flux term $S_h = 2.0 \times 10^{-3}$ is the surface roughness or the aerodynamic transfer coefficient, $\rho_a = 1.0$ kg m$^{-3}$ is the atmospheric density, $c_a = 1004$ J kg$^{-1}$ K$^{-1}$ is the specific heat capacity of the air and $U$ is the wind speed over the surface of the volcano. In this equation the diffusion of thermal energy up through the matrix and magmatic gas is balanced by the radiative transfer of energy to and from the atmosphere, and a sensible heat flux (atmospheric convection due to wind across the lava dome surface).

[25] Heat is advected upward the dome by the magmatic gas flux. Hence there is also an advective gas flux away from the lava dome surface as heat is carried by the escaping magmatic gas [*Carn et al.*, 2004]. This term could be included on the right-hand side of equation (5). However, in the lava dome interior there is also an advective heat flux to the surface in the magmatic gas. This term would be written on the left-hand side of equation (5). The mass of magmatic gas crossing the lava dome surface is conserved, and the temperature of the magmatic gas is continuous across the interface. Hence the advective heat flux due to the magmatic gas escaping from the surface is equal to the heat flux from below, and these two advective heat fluxes cancel (see Figure 1). This means that the advection of heat by magmatic gases does not contribute directly to the surface energy balance. However, it has a direct impact on the interior temperature profile, which then governs the surface temperature, and the loss of energy to the atmosphere via the radiative and convective (sensible) heat fluxes in equation (5).

[26] Boundary conditions are also required at the bottom of the carapace region. At a level $\tilde{z} = -L$ (the bottom of the rigid carapace), the temperature is maintained at $\tilde{T}(\tilde{z} = -L, t) = 1100$ K, the andesite temperature at depth inferred by *Barclay et al.* [1998]. Additionally, further conditions on density are required at $\tilde{z} = -L$. In the steady state model the mass flux is constant and in the time-dependent model the density gradient is constant (with the exception of the investigation into the forced mass flux variation at depth).

## 2.4. Nondimensionalization of Model Equations

[27] To assist analysis of this model it is first nondimensionalized. The thermal boundary layer is assumed to have thickness $L$ and this is used to nondimensionalize the length scales in the model, with the nondimensional (careted) spatial coordinate $\hat{z}$ satisfying $\hat{z} = \tilde{z}/L$. The advective timescale for the magmatic gas flux is used to nondimensionalize time. The nondimensional timescale $\hat{t}$ is

$$\hat{t} = [v_g]\tilde{t}/L, \tag{6}$$

where $[v_g]$ is a typical value for the magmatic gas mass flux. Properties of the magmatic gas and the lava dome temperature vary across the thermal boundary layer. This motivates nondimensional forms for magmatic gas pressure ($\hat{p}_g$), density ($\hat{\rho}_g$) and temperature ($\hat{T}$) which are related to their dimensional counterparts through

$$\tilde{p}_g = p_a + [p_g]\hat{p}_g, \tag{7}$$

$$\tilde{T} = T_a + [T]\hat{T}, \tag{8}$$

$$\tilde{\rho}_g = \rho_{g_a} + [\rho_g]\hat{\rho}_g, \tag{9}$$

where the dimensional scale for pressure $[p_g]$ is the difference between the atmospheric pressure $p_a = 9 \times 10^5$ Pa at the surface and the pressure at level $\tilde{z} = -L$ necessary to drive a mass flux per unit cross-sectional area of $m_g$ through a dome. Similarly, the dimensional scale for temperature $[T] = 802$ K is the difference between the atmospheric temperature $T_a = 298$ K and the temperature at level $\tilde{z} = -L$, which is $\tilde{T}(\tilde{z} = -L, t) = 1100$ K. The dimensional scale for the magmatic gas density $[\rho_g]$, is the difference in magmatic gas density as a parcel of magmatic gas is moved from $\tilde{z} = -L$ to the surface, where it is subjected to atmospheric pressure and temperature. With this scaling for the magmatic gas density, the ideal gas equation defines $\rho_{ga}$ through

$$\rho_{g_a} = \frac{p_a}{\mathcal{R}_g T_a}. \tag{10}$$

Similarly, the ideal gas equation can be used to relate the dimensional scales themselves through

$$[p_g] = [\rho_g]\mathcal{R}_g[T], \tag{11}$$

This means the nondimensional ideal gas equation has the form

$$\hat{p}_g = \Theta\hat{\rho}_g + \delta\hat{T} + \hat{\rho}_g\hat{T}, \tag{12}$$

where

$$\Theta = \frac{T_a}{[T]} = 0.372, \tag{13}$$

$$\delta = \frac{\rho_{g_a}}{[\rho_g]} = 3.34. \tag{14}$$

[28] As well as choosing the temperature scale across the thermal boundary layer it is convenient to specify the mass flux of magmatic gas across the thermal boundary layer

$$m_g = \phi[\rho_g][v_g] = \frac{\mathcal{K}[p_g]^2}{\mu_g L \mathcal{R}_g[T]}, \tag{15}$$

where $\tilde{v}_g = [v_g]\hat{v}_g$ and $[v_g] = \mathcal{K}/\mu_g\phi$ is the typical dimensional scale for the velocity. This is chosen to balance the volume flux with the pressure gradient in Darcy's law (equation (3)). Combining (15) and (11) gives a typical pressure scale across the thermal boundary layer necessary to drive any prescribed mass flux through the pore spaces of the lava dome.

[29] Having specified the dimensional scales in the problem they are substituted into the field equations giving nondimensional conservation laws for energy, mass, and momentum. These are

$$\frac{\partial}{\partial\hat{t}}\left[\left\{1 + \varepsilon\left(\delta + \hat{\rho}_g\right)\right\}\hat{T}\right] + \varepsilon\frac{\partial}{\partial\hat{z}}\left\{\left(\delta + \hat{\rho}_g\right)\hat{v}_g\hat{T}\right\} - \frac{1}{Pe}\frac{\partial^2\hat{T}}{\partial\hat{z}^2} = 0, \tag{16}$$

$$\frac{\partial\hat{\rho}_g}{\partial\hat{t}} + \frac{\partial}{\partial\hat{z}}\left[\left(\delta + \hat{\rho}_g\right)\hat{v}_g\right] = 0, \tag{17}$$

and

$$\hat{v}_g = -\frac{\partial\hat{p}_g}{\partial\hat{z}_g} - \beta\left(\delta + \hat{\rho}_g\right), \tag{18}$$

respectively, where the nondimensional numbers present in this system of equations are

$$\beta = \frac{[\rho_g]Lg\cos\alpha}{[p_g]}, \tag{19}$$

$$\varepsilon = \frac{\phi c_g[\rho_g]}{(1 - \phi)c_r\rho_r}, \tag{20}$$

corresponding to the ratio of the pressure gradient to the effect of gravity in Darcy's law and the ratio of the specific

**Table 3.** Values of Nondimensional Numbers in the Model for $L = 20$ m and $m_g = 3.5 \times 10^{-3}$ kg s$^{-1}$ m$^{-2}$ [a]

| Symbol | Value | Nondimensional Number | Equations |
|--------|-------|------------------------|-----------|
| $\Theta$ | 0.372 | ratio of atmospheric temperature to temperature difference across thermal boundary layer | (13) |
| $\delta$ | 1.10 | ratio of atmospheric density to density difference across thermal boundary layer | (14) |
| $\beta$ | $5.31 \times 10^{-4}$ | influence of gravity on the magmatic gas | (19) |
| $\varepsilon$ | $1.16 \times 10^{-4}$ | ratio of magmatic gas specific heat capacity to andesite specific heat capacity | (20) |
| $Pe$ | $9.19 \times 10^{5}$ | magmatic gas Péclet number | (21) |
| $B$ | 13.7 | coefficient of radiative heat flux in thermal boundary condition | |
| $C$ | 96.4 | coefficient of convective heat flux in thermal boundary condition for a wind speed of 5 m s$^{-1}$ | |

[a]The values of the physical constants contributing to these numbers are given in Tables 1 and 2.

heats of magmatic gas to andesite, respectively. A Péclet number measures the ratio of thermal advection to thermal diffusion in the lava dome

$$Pe = \frac{[v_g]L(1-\phi)c_r \rho_r}{k_e}. \qquad (21)$$

[30] The nondimensional surface pressure and temperature are $\hat{p}_g(0, \hat{t}) = 0$ and $\hat{T}(0, \hat{t}) = \hat{T}_s(\hat{t})$ respectively and the nondimensional surface density is

$$\hat{\rho}_g(0, \hat{t}) = -\frac{\delta \hat{T}_s(\hat{t})}{\Theta + \hat{T}_s(\hat{t})}, \qquad (22)$$

while the temperature satisfies the nondimensional version of the heat flux boundary condition (5):

$$\left.\frac{\partial \hat{T}}{\partial \hat{z}}\right|_{z=0} = -\mathcal{H}(\hat{T}_s), \qquad (23)$$

where the nondimensional heat flux

$$\mathcal{H}(\hat{T}_s) = B\left(4\hat{T}_s + \frac{6\hat{T}_s^2}{\Theta} + \frac{4\hat{T}_s^3}{\Theta^2} + \frac{\hat{T}_s^4}{\Theta^3}\right) + C\hat{T}_s. \qquad (24)$$

Here $B = \epsilon_s \sigma L T_a^3 / k_e$ measures the importance of radiative cooling to a dome and $C = S_h \rho_a c_a U L / k_e$ measures the importance of convective (sensible) cooling. Notice, $C$ depends linearly on the wind speed over the lava dome surface and $S_h$, the lava dome surface roughness. This completes the nondimensionalization of the model, with typical values of the dimensionless parameters given in Table 3 for $L = 20$ m and $m_g = 3.5 \times 10^{-3}$ kg s$^{-1}$ m$^{-2}$. For these parameter values, the advective timescale for the evolution of the model, $[v_g]/L = 434.6$ seconds.

## 3. Thermal Structure of an Impermeable Lava Dome

[31] We can consider the evolution of a solid impermeable lava dome, which has no void spaces, and hence no magmatic gas flow. In this case, the energy conservation

equation (16) reduces to the nondimensional classical heat equation

$$\frac{\partial \hat{T}}{\partial \hat{t}} = \frac{1}{Pe}\frac{\partial^2 \hat{T}}{\partial \hat{z}^2}. \qquad (25)$$

An equivalent equation coupled to the boundary condition (equation (23)) was studied by *Matthews and Barclay* [2004]. In such a model, cooling continues below observed values of lava dome surface temperature on a timescale of days, leading to unrealistic predictions of the full temperature profile.

[32] Regions on the surface of a lava dome can maintain temperatures between 200 and 350°C [*Dzurisin et al.*, 1990; *Oppenheimer et al.*, 1993; *Urai*, 2000] for several months. Therefore we shall look at the steady state behavior of equation (25), in which the temperature $\hat{T} = \hat{T}(\hat{z})$, is a function of position only and does not vary with time. In this case the lava dome temperature satisfies

$$0 = \frac{\partial^2 \hat{T}}{\partial \hat{z}^2}. \qquad (26)$$

Temperature profiles resulting from equation (26) are linear functions of position, and yet must also satisfy the boundary conditions (equation (23)) and $\hat{T}(-1) = 1$. This implies the nondimensional temperature is related to the nondimensional level through

$$\hat{T} = 1 - \mathcal{H}(\hat{T}_s)(\hat{z} + 1), \qquad (27)$$

where the nondimensional surface heat flux $\mathcal{H}(\hat{T}_s)$ is given by equation (24). Here the value of the surface temperature $\hat{T}_s$ is unknown, but can be found as the smallest positive root of the quartic polynomial

$$\hat{T}_s = 1 - \mathcal{H}(\hat{T}_s). \qquad (28)$$

[33] The level $\tilde{z} = -L$ here marks the transition between the surface carapace region and the lower isothermal part of the dome (at 1100 K). Therefore the steady state surface temperature can be calculated as a function of the carapace thickness $L$ (Figure 2). Typical measurements of the lava dome carapace thickness suggest values of $L$ between 10 and 30 m [*Iverson*, 1990]. However, this purely diffusive model only predicts physically realistic lava dome surface
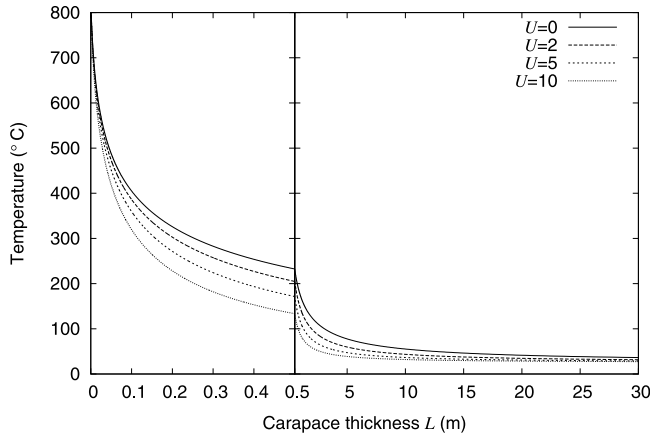
**Figure 2.** Steady state surface temperatures in an impermeable dome, as a function of carapace thickness $L$, for radiative heat fluxes only ($U = 0$) and radiative and convective heat fluxes with $U = 2$, 5, and 10 m s$^{-1}$.

temperatures above 200°C for values of $L$ less than one meter. For values of $L$ greater than 5 m, the predicted steady state surface temperature is less than 100°C regardless of the wind speed over the dome. This discrepancy illustrates that equation (25), a purely diffusive model of lava dome cooling, neglects some physical process which acts to heat the lava dome carapace. In the next section we show that thermal advection by the magmatic gas is the missing heat transfer mechanism.

## 4. Steady State Thermal Structure of a Porous Lava Dome With Magmatic Gas Flow

[34] We now seek a model of the thermal structure of a lava dome in which heat advection in the flux of magmatic gases through the void spaces is included. Initially, we look for steady states profiles of $\hat{T}(\hat{z})$, $\hat{v}_g(\hat{z})$, $\hat{p}_g(\hat{z})$ and $\hat{\rho}_g(\hat{z})$. In the steady state, derivatives with respect to time disappear, so equations (16), (17), and (18) reduce to

$$\varepsilon \frac{\partial}{\partial \hat{z}} \left\{ \left( \delta + \hat{\rho}_g \right) \hat{v}_g \hat{T} \right\} = \frac{1}{Pe} \frac{\partial^2 \hat{T}}{\partial \hat{z}^2}, \tag{29}$$

$$\frac{\partial}{\partial \hat{z}} \left[ \left( \delta + \hat{\rho}_g \right) \hat{v}_g \right] = 0, \tag{30}$$

$$\hat{v}_g = -\frac{\partial \hat{p}_g}{\partial \hat{z}} - \beta \left( \delta + \hat{\rho}_g \right), \tag{31}$$

respectively. Immediately, as a result of the nondimensionalization, the steady state mass conservation (equation (30)) is integrated to give $(\delta + \hat{\rho}_g)\hat{v}_g = 1$. Hence the steady state energy conservation (equation (29)) is reduced to an equation involving only temperature:

$$\varepsilon \frac{\partial \hat{T}}{\partial \hat{z}} - \frac{1}{Pe} \frac{\partial^2 \hat{T}}{\partial \hat{z}^2} = 0. \tag{32}$$

Temperature profiles generated by this equation are exponential functions of $\hat{z}$ and once again they must satisfy the boundary conditions (equation (23)) and $\hat{T}(-1) = 1$. For

notational brevity $\omega \equiv \varepsilon Pe$ and from equation (32) and the boundary conditions we find that the steady state temperature profile is

$$\hat{T}(\hat{z}) = 1 - \omega^{-1}\mathcal{H}\big(\hat{T}_s\big)\big(e^{\omega\hat{z}} - e^{-\omega}\big), \tag{33}$$

for $\hat{z} \leq 0$. Notice, as in the purely diffusive model, equation (33) depends on the surface temperature $\hat{T}_s$. This is given by the smallest positive root of the quartic equation

$$\hat{T}_s = 1 - \omega^{-1}\mathcal{H}\big(\hat{T}_s\big)(1 - e^{-\omega}), \tag{34}$$

by which the full profile is recovered.

[35] The steady state temperature profile depends (through $Pe$) on $m_g$, the mass flux per unit surface area of lava dome, with the relationship between $[v_g]$ and $m_g$ being given by equation (15). For "standard values" of carapace thickness with $L = 20$ m, a mass flux $m_g = 3.5 \times 10^{-3}$ kg s$^{-1}$ m$^{-2}$, and surface wind speed $U = 5$ m s$^{-1}$, the surface temperature predicted in steady state is 210°C, which is in excellent agreement with the observed temperature range of 200–350°C [*Dzurisin et al.*, 1990; *Oppenheimer et al.*, 1993]. Variations in these parameters produce a range of steady state surface temperatures (and interior profiles). Typical carapace thicknesses for lava domes have been measured at 10 to 30 m by *Iverson* [1990]. The maximum wind speed experienced around the Soufrière Hills Volcano dome is up to 35 m s$^{-1}$, which would occur during the passage of a strong hurricane. However, we are interested in the typical steady state profiles through the dome and therefore we consider the effect of a much slower wind speed of 5 m s$^{-1}$, which is typical of wind speeds measured by a nearby automated weather station [*Edmonds et al.*, 2003a]. As with the purely diffusive model shown in Figure 2, increase in wind speed above this value will lower the steady state surface temperature. The time-dependent surface temperature variation resulting from wind speed increases associated with the passage of a hurricane will be discussed in section 6.1. Variability is also present in the magmatic gas mass flux per unit surface area of lava dome, resulting from variation in the total gas mass flux, the size and surface area of the lava dome, and the effective region through which gas is emitted. The total gas mass flux of 217 kg s$^{-1}$ and dome surface area of 494000 m$^2$, reported by *Carn et al.* [2004] for Soufrière Hills Volcano on 20 March 2000 corresponds to a spatially uniform mass flux per unit surface area of $4.4 \times 10^{-4}$ kg s$^{-1}$ m$^{-2}$ (and a corresponding steady state surface temperature of just 65°C). However, neither the gas flux nor the surface temperature are uniformly distributed across the surface of a lava dome, with regions of lava dome cooler than this and temperature hot spots consistent with values recorded by *Dzurisin et al.* [1990] and *Oppenheimer et al.* [1993].

[36] Figure 3 illustrates the change in the steady state surface temperature as $m_g$, $L$ and $U$ are varied. An increase in $m_g$ leads to an increase in the predicted steady state surface temperatures $\hat{T}_s$. This is due to the increased gas mass flux, advecting additional thermal energy to the upper reaches of the lava dome. In the limit $m_g \to 0$, our new model of the thermal structure of the lava dome carapace simplifies to the purely diffusive model of an impermeable
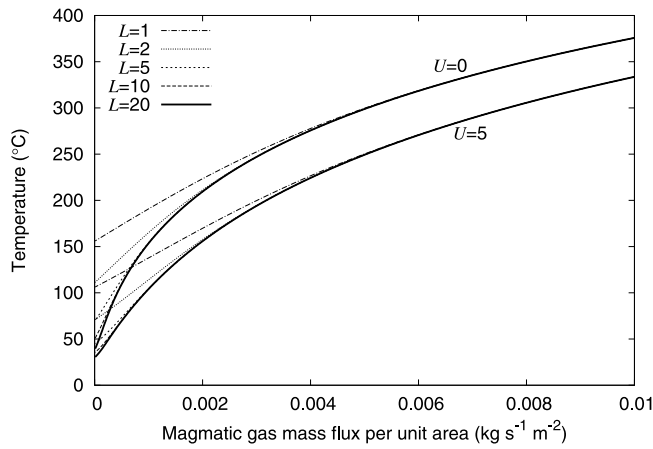
**Figure 3.** Steady state surface temperature in a permeable dome, as a function of magmatic gas mass flux per unit area. Carapace thickness of $L = 1, 2, 5, 10,$ and $20$ m, with the temperature maintained at 1100 K below the carapace.

matrix described in section 3. The steady state surface temperatures predicted in the limit $m_g \rightarrow 0$, for different choices of $L$ are the same as those given in Figure 2. The resulting steady state surface temperatures are shown for carapace thicknesses of $L = 1, 2, 5, 10,$ and $20$ m and for surface wind speeds of $U = 0$ and $5$ m s$^{-1}$. In the absence of a sensible heat flux from the surface, corresponding to no wind over the lava dome ($C = 0$ in 24), heat is transferred into the atmosphere by the thermal boundary condition solely as the result of radiation. The addition of heat transfer by atmospheric convection forced by a wind of $5$ m s$^{-1}$ lowers the steady state surface temperature by approximately 50°C, when compared to the purely radiative case. However, for typical $m_g$ both models of surface heat flux correspond to physically realistic steady state surface temperatures.

[37] For realistic values of $m_g$ the model is not strongly sensitive to the choice of $L$. *Iverson* [1990] reports solid carapace thicknesses for Mount St. Helens in the range of 10 to 30 m. Figure 3 shows that for a typical value of $m_g = 3.5 \times 10^{-3}$ kg s$^{-1}$ m$^{-2}$ the steady state lava dome temperature is nearly the same for the values of $L$ illustrated. At constant $m_g$, the steady state surface temperature remains unchanged even if $L$ is increased significantly. The reason for this can be seen by looking at the full temperature profile right across the carapace.

[38] The full steady state temperature profiles for $L = 20$ m and for a range of mass fluxes are shown in Figure 4a. These profiles exhibit thermal boundary layers (due to the
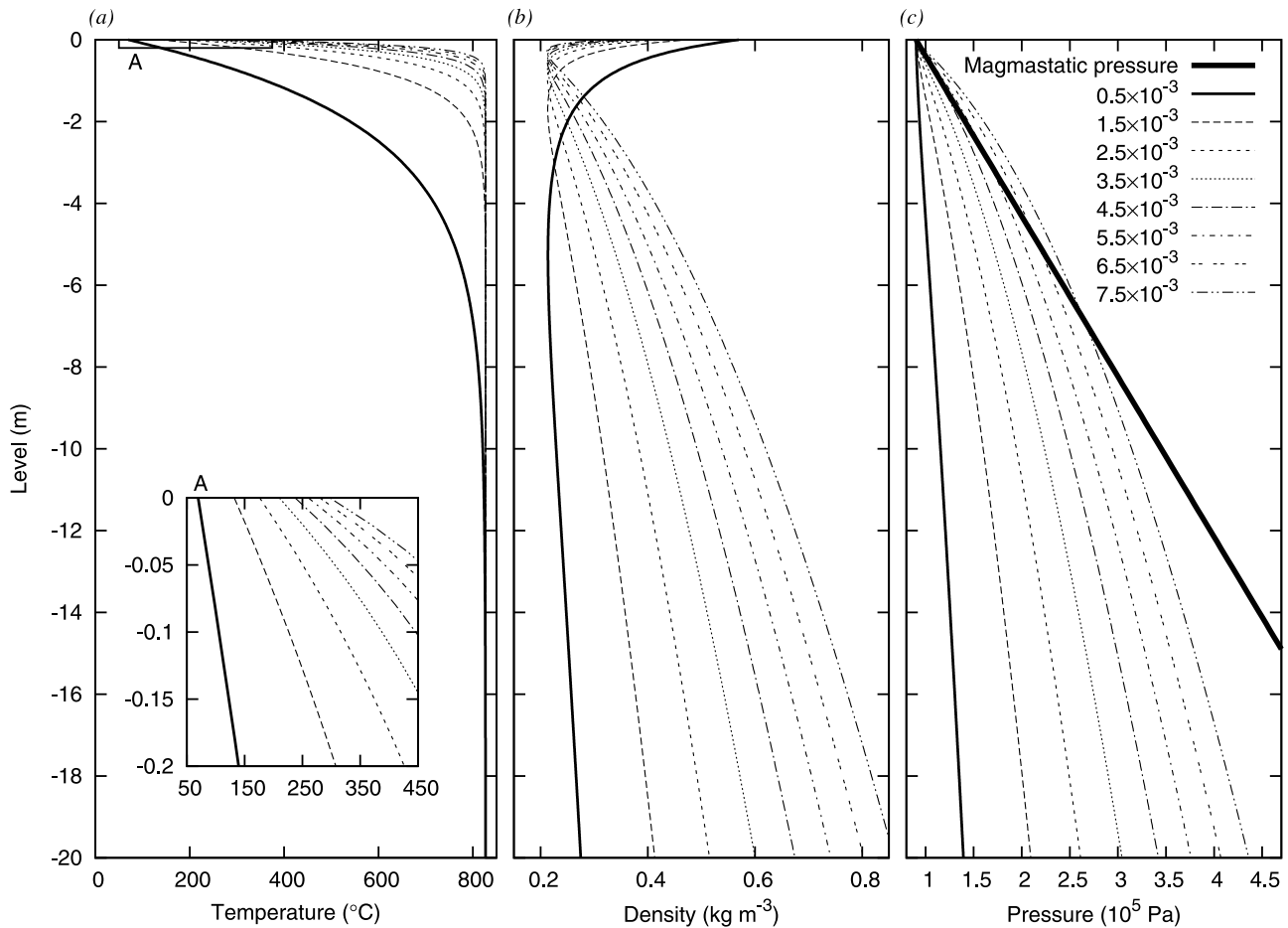


**Figure 4.** Steady state profiles for (a) temperature, (b) gas density, and (c) total gas pressure as a function of level for magmatic gas mass fluxes per unit area between $0.5 \times 10^{-3}$ (solid thick line) and $7.5 \times 10^{-3}$ kg m$^{-2}$ s$^{-1}$ in increments of $1.0 \times 10^{-3}$ kg m$^{-2}$ s$^{-1}$. The inset in Figure 4a shows the detail of the temperature profile just below the surface at $z = 0$.

exponential form of equation (33)), with the most rapid variations in temperature occurring just below the lava dome surface. In addition to predicting physically realistic lava dome surface temperatures, the thermal boundary layer in the temperature profiles indicates that if the top meter of the matrix is removed (say as the result of a small rockfall), then the temperature of the freshly exposed magma can easily reach 600–830°C. This is also consistent with visual observations of incandescence after the removal of roughly a meter of material from the actual lava dome surface [*Sparks et al.*, 2000; *Watts et al.*, 2002]. The temperature profile illustrates why the model is insensitive to the value of $L$: the thickness of the thermal boundary layer is significantly less than the value of $L$ chosen for realistic mass fluxes. Below the thermal boundary layer the temperature profiles predicted by equation (33) are approximately isothermal. This indicates that including thermal advection in the magmatic gas is sufficient to maintain realistic steady state surface temperatures even if below the level $\tilde{z} = -L$, beneath the rigid carapace the matrix does not convect in order to maintain a constant temperature at the bottom of the carapace.

[39] In steady state we can also calculate profiles for magmatic gas pressure, density, and volume flux. The total mass flux per unit area through a dome is constant $(\delta + \hat{\rho}_g)\hat{v}_g = 1$. For small $\beta$ (as defined by equation (19)), it can be shown (see Appendix A) that an analytical form exists for the density profile, which is given by

$$\hat{\rho}_g = -\delta + \frac{\sqrt{2\omega^{-2}\mathcal{H}(T_s)e^{\omega\hat{z}} + a + b\hat{z}}}{\Theta + \hat{T}}, \qquad (35)$$

where

$$a = \left(\delta + \hat{\rho}_{g,s}\right)^2(\Theta + T_s)^2 - 2\omega^{-2}\mathcal{H}(T_s), \qquad (36)$$

$$b = -2\left(\Theta + 1 + \omega^{-1}\mathcal{H}(T_s)e^{-\omega}\right), \qquad (37)$$

and the magmatic gas density at the surface $\hat{\rho}_{g,s}$, can be found by evaluating equation (12) at the surface and it is given by

$$\hat{\rho}_{g,s} = -\frac{\delta\hat{T}_s}{\Theta + \hat{T}_s}. \qquad (38)$$

For a carapace thickness $L = 20$ m and a magmatic gas mass flux $m_g = 3.5 \times 10^{-3}$ kg s$^{-1}$ m$^{-2}$, we find $\beta = 5.31 \times 10^{-4}$. The nondimensional parameter $\beta$ (defined by equation (19)) measures the relative importance of gravity to magmatic gas pressure gradient on the magmatic gas flux. The small value of $\beta$ indicates we should expect the magmatic gas flux to be largely driven by the magmatic gas pressure gradient with the influence of gravity being largely insignificant. This can be confirmed by comparing the analytical $\beta = 0$, magmatic gas density profile (equation (35)), to the numerically calculated magmatic gas density profile with $\beta = 5.31 \times 10^{-4}$. It can also be shown [*Hicks*, 2008] that the two

magmatic gas density profiles are in excellent agreement with each other. For all carapace thicknesses and magmatic gas fluxes of interest, $\beta \ll 1$ and consequently we subsequently neglect the influence of gravity on the magmatic gas mass flux.

[40] Figure 4b shows the resulting steady state magmatic gas density profiles for $L = 20$ m corresponding to the same range of $m_g$ as that used in Figure 4a. Density profiles have a minimum below the lava dome surface, the value and position of which is a function of the magmatic gas mass flux through the dome. Having calculated the magmatic gas density we can find the magmatic gas volume flux using $(\delta + \hat{\rho}_g)\hat{v}_g = 1$. Necessarily, each profile of magmatic gas *volume* flux has a maximum at the same level as the minimum in the density profile. Clearly, the magmatic gas *mass* flux is the same at all levels. Finally, using the magmatic gas density profile and the lava dome temperature we can calculate the magmatic gas pressure using equation (12). The corresponding pressure profiles are shown in Figure 4c. Pressure profiles are monotonic, with everywhere a pressure gradient driving magmatic gas upward through the dome and out into the atmosphere. For fixed values of porosity and permeability, an increase in the steady state magmatic gas mass flux per unit surface area of lava dome produces an increase in the magmatic gas pressure gradient. Hence for the standard parameter values of $m_g = 3.5 \times 10^{-3}$ kg s$^{-1}$ m$^{-2}$, and $L = 20$ m, the magmatic gas pressure is $3.04 \times 10^5$ Pa (three times atmospheric pressure) at a level 20 m below the dome surface. Note that this value is approximately 60% of the value of the magmastatic pressure of $\rho_r g\tilde{z} = 5.10 \times 10^5$ Pa (thick line in Figure 4c). Hence the internal gas pressure in this steady state are comparable to the weight of overlying rock. If the magmatic gas mass flux through the matrix is increased further, then the magmatic gas pressure exceeds the magmastatic overburden pressure in a region just below the surface. If the magmatic gas pressure exceeds the magmastatic overburden pressure plus (the harder to estimate) dome-scale tensile strength of the matrix, then it is possible that the dome matrix may sustain damage. This could widen the cracks through the dome and increase the porosity. Eventually, if sufficient damage to the matrix occurs, dome failure could be expected.

## 5. Multiple-Scale Analysis

[41] The key parameters which determine the multiple timescale behavior of a lava dome are $\varepsilon$ and $1/Pe$. In section 3 it was shown that taking the limit of $\varepsilon \to 0$ with $1/Pe \neq 0$ leads to a model of a lava dome which cools unrealistically quickly. Therefore models in which both $\varepsilon$ and $1/Pe$ are small, and of a similar order of magnitude are considered (see Table 3). We take $Pe^{-1} = A\varepsilon$, where $A = O(1)$, which allows a multiscale response of this system in two disparate timescales. Following the standard multiscale analysis [e.g., *Hinch*, 1991] we can look for the multiscale evolution of the model equations by letting physical properties such as temperature satisfy

$$\hat{T}(\hat{z}, \hat{t}) = \hat{T}(\hat{z}, \hat{t}_s, \hat{t}_f), \qquad (39)$$

for two separate timescales:

$$\hat{t}_f = \hat{t}, \tag{40}$$

a fast $O(1)$ timescale and

$$\hat{t}_s = \varepsilon \hat{t}, \tag{41}$$

a slow $O(\varepsilon^{-1})$ timescale. With $L = 20$ m and $m_g = 3.5 \times 10^{-3}$ the corresponding fast timescale $\hat{t}_f = 434.6$ seconds and the slow timescale $\hat{t}_s = 43.2$ days.

[42] Derivatives with respect to time can be expressed as

$$\frac{\partial}{\partial \hat{t}} = \left(\frac{\partial}{\partial \hat{t}_f}\right)_{\hat{t}_s} + \varepsilon \left(\frac{\partial}{\partial \hat{t}_s}\right)_{\hat{t}_f}. \tag{42}$$

We now substitute this relationship into equations (17) and (16), and look for regular perturbation expansions of the form $\hat{\gamma} = \hat{\gamma}_0 + \varepsilon \hat{\gamma}_1 + \varepsilon^2 \hat{\gamma}_2 + \cdots$, where the symbol $\hat{\gamma}$ is successively $\hat{T}$, $\hat{v}_g$, $\hat{p}_g$ and $\hat{\rho}_g$. Matching the coefficients of $\varepsilon$ at leading order governs the behavior of the system on the fast timescale

$$\frac{\partial \hat{\rho}_{g,0}}{\partial \hat{t}_f} - \frac{\partial}{\partial \hat{z}}\left[\left(\delta + \hat{\rho}_{g,0}\right)\frac{\partial \hat{p}_{g,0}}{\partial \hat{z}}\right] = 0, \tag{43}$$

$$\frac{\partial \hat{T}_0}{\partial \hat{t}_f} = 0. \tag{44}$$

Equation (43) states that while the density can evolve on the fast timescale (as in the full system), the temperature in equation (44) is unchanged on this fast timescale. Therefore changes in temperature only occur over the much longer $\hat{t}_s$-timescale. To investigate temperature variations analytically, higher order terms in the perturbation expansion must be considered. Rather than undertaking this very complicated analysis, the full system is investigated numerically, in section 6. Theoretically, variations in lava dome temperatures will only occur over much longer timescales than variations in magmatic gas volume flux, pressure, and density.

## 6. Time-Dependent Perturbations of a Porous Lava Dome

[43] To investigate the relative lengths of the fast magmatic gas timescale and the slow temperature evolution timescale, we shall conduct three numerical investigations corresponding to physically realistic perturbations of a lava dome. In the next three subsections, we shall explore sequentially the effects of an atmospheric pressure variation, a small rockfall from the dome surface, and a change in magmatic gas mass flux at depth upon the steady state lava dome temperature profile.

[44] To rewrite the system of equations in a form amenable to numerical analysis, we shall work solely in the small $\beta$ limit and assume the role of gravity has a negligible impact on the magmatic gas flux. The equations are investigated using a standard finite difference procedure on a regular grid with 250 points. In the dimensional

coordinate system with $L = 20$ m this corresponds to one grid point every 8 cm across the dome carapace.

[45] Before perturbing the steady state profile, the analytically predicted profiles are run through the time-dependent code for a period of 20 model days to generate numerically stabilized profiles. These numerically stabilized profiles differ slightly from the analytical predictions of the steady states, given by equations (33) and (35), with the maximum variation occurring in the temperature profile just below the surface, where the large temperature gradients make the finite difference approximation least accurate. The numerically stabilized surface temperature is typically 2% higher than that predicted by the analytical steady state profile. This numerically stabilized profile is then used as the initial profile for the subsequent perturbations.

### 6.1. Influence of the Passage of a Low-Pressure Weather System

[46] Volcanic activity has been reported to be influenced by atmospheric pressure variations at Pavlof Volcano in the Aleutian Islands on timescales of a year [McNutt and Beavan, 1987; McNutt, 1999] and at Stromboli Volcano, Italy over timescales of a few hours [Neuberg, 2000]. This motivates the question: what is the characteristic response of a lava dome to atmospheric modulation? Our primary case study is the Soufrière Hills Volcano in the Caribbean, a region frequently affected by hurricanes. As an idealized example the effect of the pressure variation associated with the passage of a hurricane over the lava dome is investigated. Surface pressure variations alone will be considered and the effect of increased wind speed and surface sensible heat flux, and significant rainfall (which often accompanies hurricanes) will not be included. Modeling the effect of rainfall adds significant additional complexity and is not included here [Taron et al., 2007; Hicks, 2008], although its effect on lava dome stability are significant [Mastin, 1994; Yamasato et al., 1998; Matthews et al., 2002; Carn et al., 2004].

[47] The passage of the low-pressure weather system is modeled by assuming a new dimensional surface pressure $\tilde{p}_{g,s}(\tilde{t})$ which changes over time, decreasing from a constant atmospheric pressure $p_a$ and returning to $p_a$ after time $\mathcal{T}$.

$$\tilde{p}_{g,s}(\tilde{t}) = \begin{cases} p_a - \dfrac{\Delta p_g}{2}\left(1 - \cos\left(\dfrac{2\pi\tilde{t}}{\mathcal{T}}\right)\right), & 0 \leq \tilde{t} \leq \mathcal{T}, \\ p_a, & \text{otherwise}, \end{cases}$$

where $\Delta p_g$ is the amplitude of the variation from atmospheric pressure and $\mathcal{T}$ is the length of time it takes for the hurricane to pass over the lava dome and the atmospheric pressure to return to its original value. This section shows results from a typical model run for a very strong hurricane that takes $\mathcal{T} = 12$ hours to pass over the volcano, with $p_a = 90000$ Pa at 1000 m elevation, and a minimum pressure $p_a - \Delta p = 80000$ Pa.

[48] Figure 5a shows the evolution of the pressure at the surface. The resulting disturbance in the dome interior magmatic gas pressure (Figure 5b) closely follows the perturbation of atmospheric pressure. In Figure 5b, the absence of a visible lag between the perturbation and the resulting disturbance indicates that the pressure varies rapidly in response to the surface pressure perturbation, with
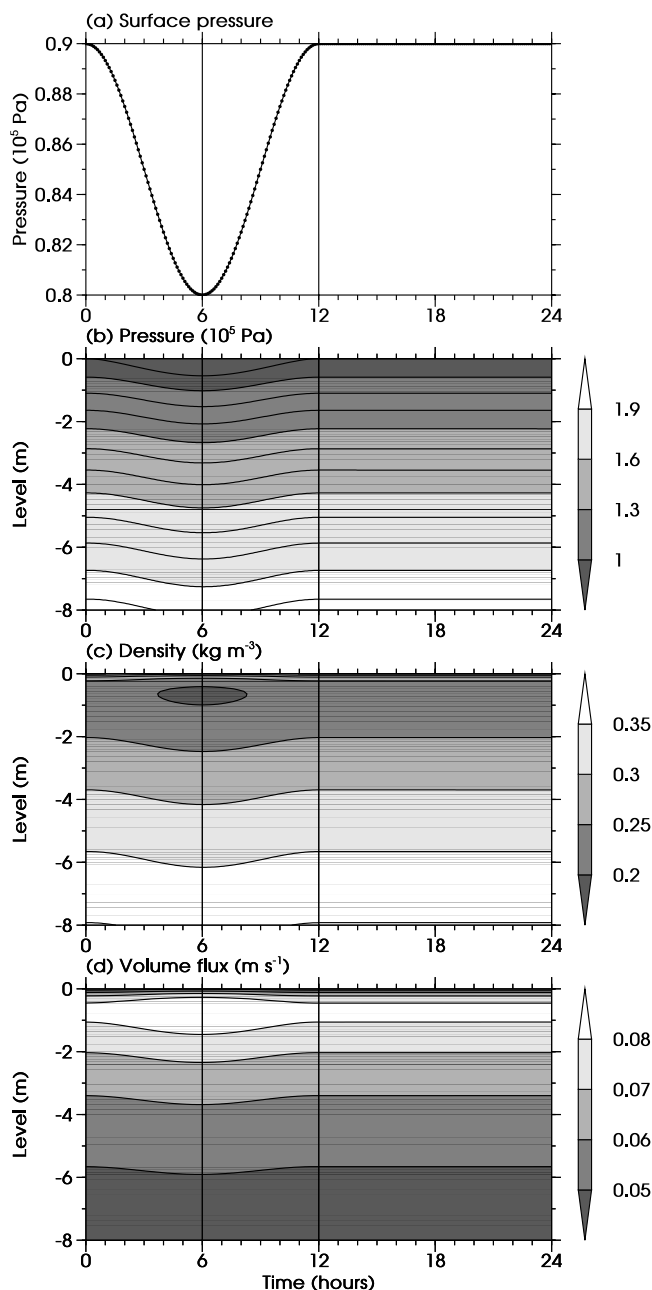
**Figure 5.** Evolution of lava dome, as a dry, low pressure weather system with a minimum pressure of 80,000 Pa moves over the summit of the volcano. (a) Surface pressure (in $10^5$ Pa), (b) pressure with contours every $0.1 \times 10^5$ Pa, (c) magmatic gas density with contours every 0.05 kg m$^{-3}$, and (d) magmatic gas volume flux per unit surface area with contours every 0.01 m s$^{-1}$. See legends for shading.

information transmitted over a short timescale of the order of a few minutes. The deviation from the steady state profile decreases with depth, indicating that the disturbance is localized close to the dome surface. The corresponding variations in the profiles of $\rho$ and $v$ are shown in Figure 5c and Figure 5d, respectively. Again, we see that the variations in density and magmatic gas volume flux last as long as the variation in the surface pressure, with the greatest disturbances occurring just below the dome surface.

This indicates that, like the pressure, variations in density and volume flux are transmitted over the short timescale of a few minutes.

[49] The evolution of the temperature (Figure 6) is markedly different to the profiles of pressure, density, and gas volume flux shown previously. Surface temperature variations are quite small, up to only 4°C. Temperature changes at depth are smaller still. The surface temperature of the dome does not return to its original value immediately after the pressure perturbation has passed over the dome: the temperature distribution is still recovering many hours after the hurricane has completely departed. Hence temperature variations occur on a much longer timescale than gas pressure, density or volume flux changes, as predicted.

[50] To study the influence of wind speed variation, a second test was run where the convective heat flux from the surface varied between 5 m s$^{-1}$ and 30 m s$^{-1}$. A sinusoidal evolution of the wind speed was used to match the pressure evolution (equation (45)) and to mimic the high winds associated with the passage of a hurricane. The increased wind speed and associated higher surface heat fluxes produced significantly greater temperature changes, with a surface temperature minimum of 110°C recorded 40 minutes after peak wind speeds. This compares with a steady state surface temperature after an indefinite period of 30 m s$^{-1}$ winds of 100°C. The surface temperature does not approach prehurricane levels until many hours after the hurricane has passes and surface pressure and wind speed are back to normal. Some changes in the pressure profiles are also evident in this period, but in this phase further pressure evolution is determined by the much slower temperature profile recovery.

### 6.2. Influence of Small Rockfalls

[51] The surface of a lava dome is unstable and affected by frequent small rockfalls. These are on a much smaller scale than dome collapse events, but locally small rockfalls allow material to be gradually removed from the surface thus exposing hotter magma from below. The effect of this on the steady state profiles described in section 4 is simulated by an idealized instantaneous removal of the top metre of rock and examination of the subsequent
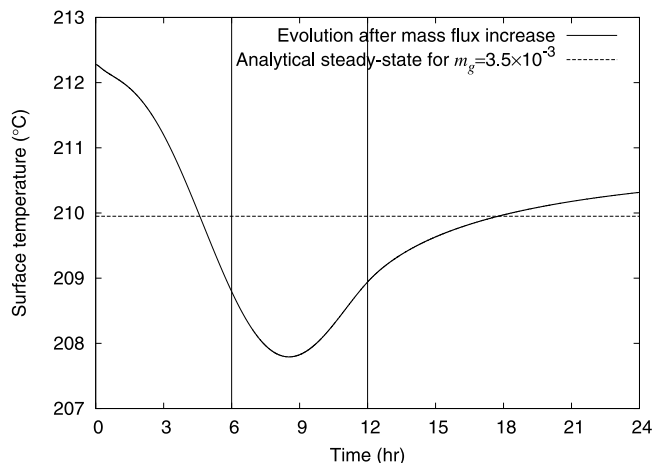


**Figure 6.** As in Figure 5, showing the evolution of lava dome surface temperature.

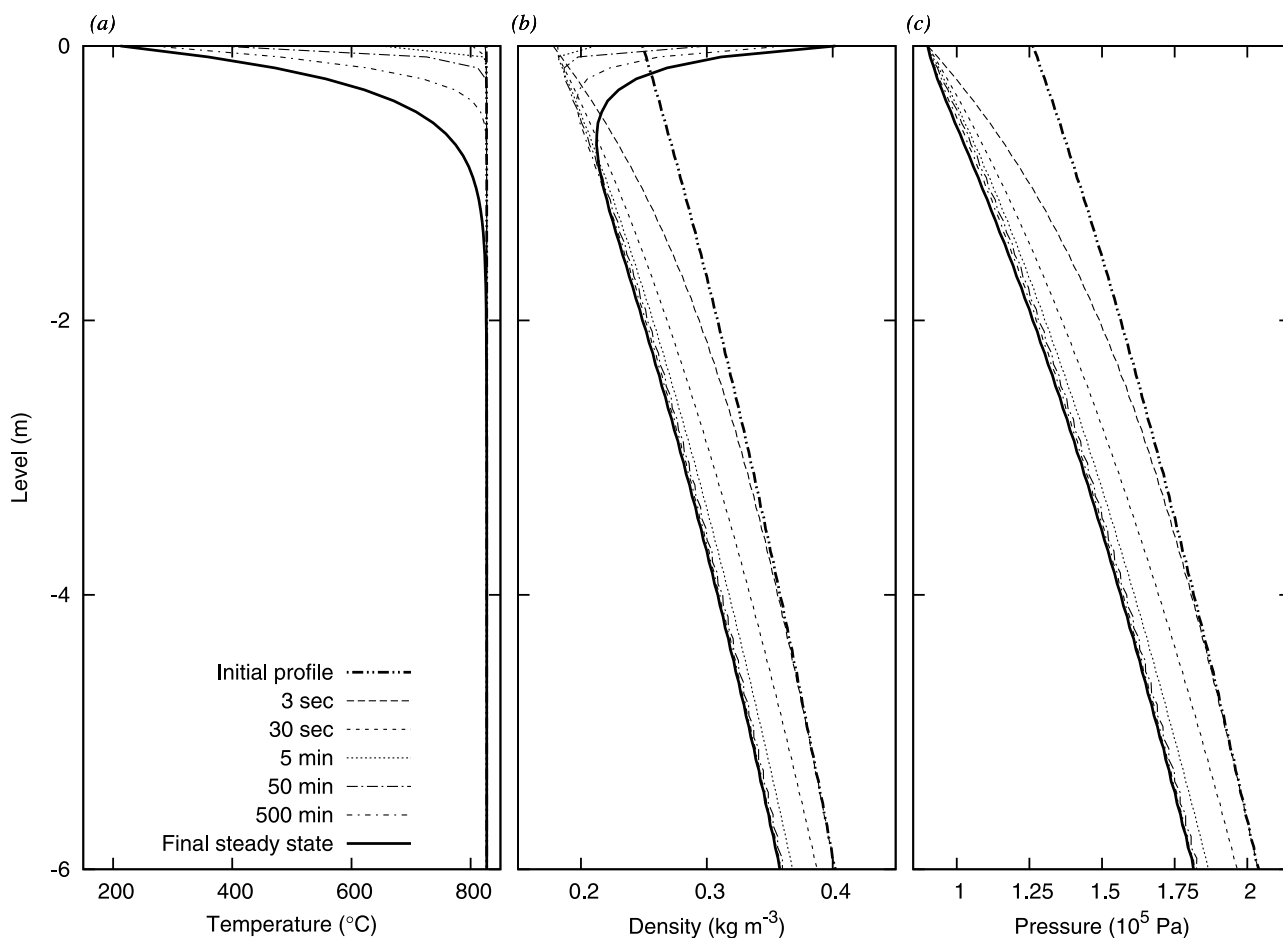**Figure 7.** Evolution of lava dome, after the top 1 m is removed due to a rockfall from the surface. (a) Temperature in °C, (b) gas density in kg m$^{-3}$, and (c) pressure in Pa at 3 seconds, 30 seconds and 5 minutes, 50 minutes, and 500 minutes after the instantaneous removal of 1 meter from the lava dome surface.

evolution of the lava dome. To justify sudden removal of rock in the model we note that rockfalls do occur on much shorter timescales than even the shortest timescale over which the magmatic gas pressure, density, and volume flux evolve.

[52] Figure 7 shows the evolution of the lava dome temperature, and magmatic gas density and pressure profiles at 3 seconds, 30 seconds, and 5, 50 and 500 minutes after the instantaneous removal of the top one metre of andesite from the dome. Two thicker lines are plotted in Figure 7, corresponding to the steady state profile prior to the rockfall (dashed) and the final steady state profile after the rockfall (solid). The removal of 1 m of andesite exposes magma with a temperature in excess of 800°C, as observed in actual rockfall events. This is a 500°C increase locally in the surface temperature.

[53] The instantaneous removal of surface rock brings about an instantaneous discontinuity in the pressure profile, as magma previously at depth is suddenly exposed on the surface. Over short timescales the pressure discontinuity is smoothed out, with the new surface pressure being carried rapidly into the dome interior, producing physically reasonable magmatic gas volume fluxes. Isopleths corresponding to magmatic gas pressure and density are shown in Figure 8. Although a lava dome surface temperature in excess of 800°C and the surface heat flux given by equation (5) results in rapid cooling, the changes in temperature again take place much more slowly than the simultaneous evolution of the magmatic gas pressure, density, and volume flux. Hence 30 minutes after the rockfall, the profile of gas pressure and density have equilibrated with the current temperature (indicated by approximately constant isopleths in Figure 8). However, the temperature profile is still adjusting as show by Figure 7. While the lava dome is cooling over several days, the magmatic gas pressure, density, and volume flux quickly adapt to the changing temperature profiles, changing on the order of a few minutes.

## 6.3. Influence of Magmatic Gas Mass Flux Variation

[54] The steady state profiles calculated in section 4 assume that the magmatic gas mass flux through the lava dome is constant. However, significant temporal variations in the magmatic gas fluxes from the Soufrière Hills Volcano have been recorded [*Edmonds et al.*, 2001]. Hence steady state solutions may not be applicable and the response to a time-dependent mass flux is investigated.
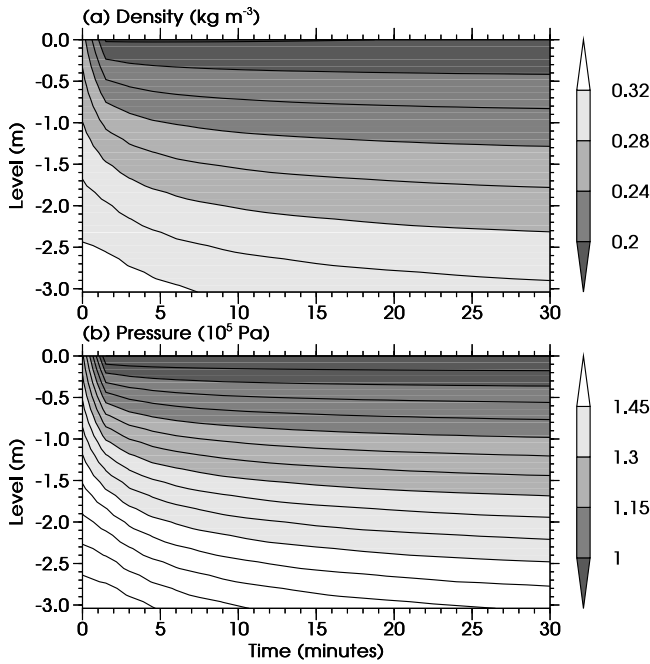
**Figure 8.** As in Figure 7. (a) Density with contours every 0.02 kg m$^{-3}$ and (b) pressure with contours every 0.05 × 10$^5$ Pa. See legends for shading.

[55] An idealized experiment is carried out, where the steady state profiles are perturbed by instantaneously increasing the magmatic gas flux per unit surface area of lava dome, 20 m below the surface, from 3.5 × 10$^{-3}$ to 5.5 × 10$^{-3}$ kg m$^{-2}$ s$^{-1}$, at $\tilde{t} = 0$. This corresponds to an increase in the steady state surface temperature from 210 to 260°C. Such an increase in mass flux could be an idealization of the effect of the system being charged with a basaltic input at depth [*Edmonds et al.*, 2001].

[56] Immediately after the mass flux is increased, there is a discontinuous jump in pressure at the lower boundary. This is shown by the rapidly changing isopleths at this point in a time-level section of density (Figure 9a) and pressure (Figure 9b). The rapidly changing isopleths are an immediate consequence of Darcy's law (equation (18)) as a greater pressure gradient is required to drive the increased mass flux up through the dome. However, by $\tilde{t} = 10$ minutes the effect of the increased mass flux through the dome has been transmitted to the surface, and the isopleths once again appear approximately constant in time, albeit with a higher pressure gradient. By this stage the changes in the pressure corresponding to the fast $\hat{t}$-timescale have been completed and any further change in pressure occurs due to the temperature evolution alone, over the much longer timescale.

[57] The analytical steady state profiles predict a lava dome surface temperature of 260°C for $m_g = 5.5 \times 10^{-3}$ kg m$^{-2}$ s$^{-1}$, which is an increase of almost 50°C from the initial surface temperature. However, 10 minutes after the instantaneous increase in $m_g$, the lava dome surface temperature has barely changed from its initial value. Figure 10 shows the surface temperature as a function of time as it varies between the two analytical steady state temperatures. Notice, in marked contrast to the magmatic gas pressure and density which evolve to quasi steady states over the fast $\hat{t}_f$
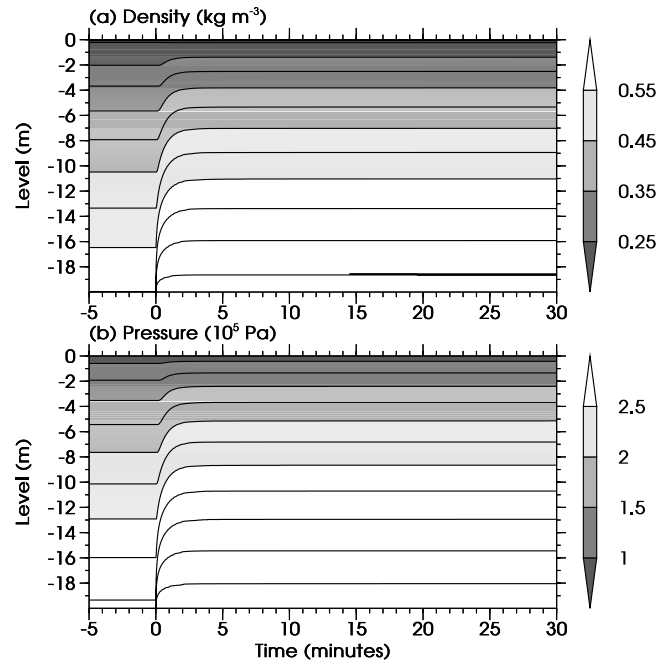


**Figure 9.** Evolution of lava dome, when at $\tilde{t} = 0$ the magmatic gas mass flux per unit area changes from 3.5 × 10$^{-3}$ to 5.5 × 10$^{-3}$ kg m$^2$ s$^{-1}$ at a depth of $\tilde{z} = -20$ m. (a) Density with contours every 0.05 kg m$^{-3}$ and (b) pressure with contours every 0.25 × 10$^5$ Pa. See legends for shading.

timescale of about 10 minutes, it takes a period of approximately 5 days (the slow $\hat{t}_s$-timescale) for the surface temperature to approach its new value. This is predicted by the analysis at the start of this section with equations (43) and (44) implying the temperature will change slowly while the magmatic gas pressure, density, and volume flux evolve much more rapidly. Over the longer timescale the magmatic gas pressure, density, and volume flux continue to change in slavish response to the very slow temperature variations.

## 7. Discussion

[58] Models of the thermal structure of a lava dome that rely solely on diffusion in the solid matrix for the transport
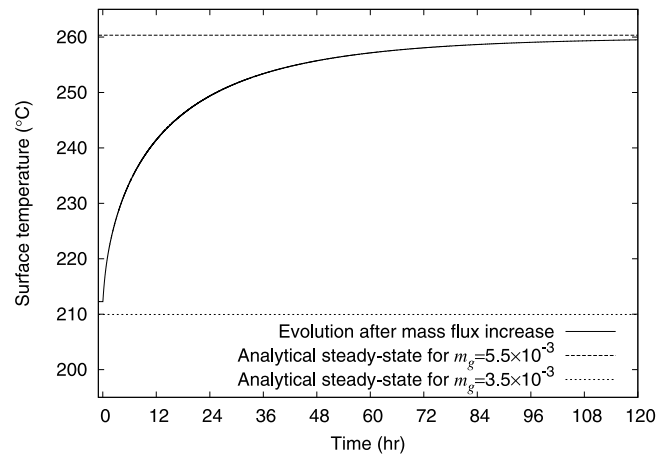


**Figure 10.** As in Figure 9, showing the evolution of lava dome surface temperature.

of heat [e.g., *Matthews and Barclay*, 2004] are shown to cool too rapidly and evolve to steady state surface temperatures significantly below observed values, unless magma is allowed to convect unrealistically close to the surface. Therefore in addition to thermal diffusion in the solid matrix, extra physical processes are required to produce realistic temperature profiles. A new model is proposed that describes the thermal structure of a lava dome, and for the first time incorporates the porosity of the andesite and the transport of mass and heat (thermal advection) by magmatic gases through the void spaces. If the model is forced with realistic gas mass fluxes rising up through the void spaces of a dome, then the resulting steady state surface temperatures are significantly higher than those predicted by thermal diffusion alone. For example, a gas mass flux per unit area of $3.5 \times 10^{-3}$ kg s$^{-1}$ m$^{-2}$ corresponds to a steady state surface temperature of $210°C$, in excellent agreement with surface temperatures observed on lava domes [*Dzurisin et al.*, 1990; *Oppenheimer et al.*, 1993; *Urai*, 2000]. Higher mass fluxes through the dome generate predictions of higher steady state surface temperatures.

[59] This motivates the intriguing question: is it possible to infer information about the mass flux of magmatic gases through a dome based on observations of the surface temperature alone? This has practical applications, as the magmatic gas flux is a controlling parameter in predicting future eruptive behavior. However, direct methods [e.g., *Edmonds et al.*, 2003a, 2003b] of measuring the magmatic gas mass flux from a dome are time consuming and require suitable atmospheric conditions. This makes it difficult to monitor of the magmatic gas mass flux continuously. That said, a forward looking infrared (FLIR) camera [*Vaughan et al.*, 2005] can record the dome surface temperature continuously, including during periods of inclement weather.

[60] Steady state calculations (Figure 3) suggest there is a relationship between the magmatic gas mass flux and the lava dome surface temperature. The model predicts that an increase in the magmatic gas mass flux from, say $3.5 \times 10^{-3}$ to $5.5 \times 10^{-3}$ kg s$^{-1}$ m$^{-2}$ should produce a corresponding increase in the lava dome surface temperature from 210 to $260°C$. Therefore if a FLIR camera monitoring a dome records a significant increase in the surface temperature over a short period of time, then this could correspond to an increase in the magmatic gas mass flux, with possible implications for the stability of the whole dome and eruptive activity. However, although there is a relationship between the surface temperature and the magmatic gas mass flux in the steady state, section 6.3 shows there is a strong timescale separation between the thermal profile in the dome (which includes the surface temperature) and the dynamic properties of the magmatic gas (including the gas mass flux) as the dome evolves toward a new steady state.

[61] A multiple-scale analysis in section 5 predicts that the surface temperature of the lava dome will evolve toward the new steady state over a period of approximately 40 days, while the magmatic gas mass flux approaches a quasi-steady state profile in approximately 10 minutes. This is confirmed by the numerical investigation in section 6.3. Additionally, one might reasonably expect that many changes in the magmatic gas might occur during a period of 40 days. Therefore the lava dome thermal profile and

magmatic gas fluxes are never in steady state. Hence quantitative predictions of the magmatic gas mass flux increase, corresponding to any recorded surface temperature increase, are difficult to obtain. Further analysis (perhaps exploiting the rate of change of the surface temperature with signal processing techniques), together with additional fieldwork studies may constrain the relationship between surface temperature and the magmatic gas mass flux, which may precede a surge in lava output or eruptive activity.

[62] However, qualitative information on large magmatic gas mass flux variations can still be gained from surface temperature monitoring. Sudden increases in the surface temperature over short periods in time should correspond to increases in the magmatic gas flux, even if the new magmatic gas flux through a dome cannot be quantified. For example, when the gas flux changes from $3.5 \times 10^{-3}$ to $5.5 \times 10^{-3}$ kg s$^{-1}$ m$^{-2}$ as part of the numerical investigation conducted in section 6.3, there is a $13°C$ increase in temperature in the first two hours after the change in the gas flux. This change in surface temperature could be recorded by a FLIR camera even if the ultimate steady state surface temperature cannot. If such a surface temperature increase is observed it could motivate taking a direct measurement of the gas flux from the dome at the earliest opportunity. Fieldwork is required in order to determine whether time series of dome surface temperature might provide an early warning mechanism, of large increases in the magmatic gas mass flux.

[63] Two other physically motivated perturbations of the steady state profile were investigated: the passage of a low pressure weather system over the summit of the volcano (section 6.1) and a small rockfall from the lava dome surface (section 6.2). They also exhibit the large timescale separation between the characteristic dynamic response of the magmatic gas and the thermal evolution of the matrix. Once again the numerical investigation of a dome evolution exhibits timescales which are in excellent agreement with the multiple scale analysis: the dynamic properties of the magmatic gas evolve over 10 minutes, while the thermal properties of a dome evolve over many days. This confirms that a large timescale separation, between the dynamic response of the magmatic gas and the thermal evolution of the dome, is likely to be a feature in all perturbations of steady state dome profiles.

[64] Further development of this theory would see the thermal and mass advection in the magmatic gas phase incorporated into existing models of lava dome growth. This necessitates that a dome be considered as a porous medium, for the first time within models of lava dome growth. If the porosity was allowed to vary (with concomitant variations in viscosity corresponding to structural weaknesses within the dome), then this combination of additional physics would be an important step toward accurately modeling exogenous lava dome growth.

## Appendix A: Steady State Density Profile Calculations

[65] In a steady state the magmatic gas mass conservation equation (30) implies $(\delta + \hat{\rho}_g)\hat{v}_g = 1$. This relationship between magmatic gas volume flux and density, together

with equations (12) and (31) can be used to generate an ordinary differential equation for $\rho$ of form

$$\frac{1}{\delta + \hat{\rho}_g} = -(\Theta + \hat{T})\frac{d\hat{\rho}_g}{d\hat{z}} - \left(\delta + \hat{\rho}_g\right)\frac{d\hat{T}}{d\hat{z}} - \beta\left(\delta + \hat{\rho}_g\right), \quad \text{(A1)}$$

in which all the other variables are known. If we define a new variable $\hat{y} = (\delta + \hat{\rho}_g)^2$, then equation (A1) is transformed into a nonlinear Bernoulli ordinary differential equation, the solution of which is given by

$$\frac{d}{d\hat{z}}\left[\hat{y}\hat{f}\right] = -\frac{2\hat{f}}{\Theta + \hat{T}}, \quad \text{(A2)}$$

where $\hat{f}$ is an integrating factor and depends upon the level $\hat{z}$ through

$$\hat{f} = \exp\left[\int \frac{2}{\Theta + \hat{T}}\left(\frac{d\hat{T}}{d\hat{z}} + \beta\right)d\hat{z}\right]. \quad \text{(A3)}$$

Having substituted for the temperature profile from equation (33), the resulting integral (equation (A2)) has no analytical solution except in the special case of $\beta = 0$. The nondimensional analytical density profile for $\beta = 0$ is given by

$$\hat{\rho}_g = -\delta + \frac{\sqrt{2\omega^{-2}\mathcal{H}(T_s)e^{\omega\hat{z}} + a + b\hat{z}}}{\Theta + \hat{T}}, \quad \text{(A4)}$$

where

$$a = \left(\delta + \hat{\rho}_{g,s}\right)^2(\Theta + T_s)^2 - 2\omega^{-2}\mathcal{H}(T_s), \quad \text{(A5)}$$

$$b = -2\left(\Theta + 1 + \omega^{-1}\mathcal{H}(T_s)e^{-\omega}\right), \quad \text{(A6)}$$

and the magmatic gas density at the surface $\hat{\rho}_{g,s}$, can be found by evaluating equation (12) at the surface and is given by

$$\hat{\rho}_{g,s} = -\frac{\delta \hat{T}_s}{\Theta + \hat{T}_s}. \quad \text{(A7)}$$

For typical parameter values $\beta = 2.65 \times 10^{-4}$ and the numerical solution of equation (A1) gives excellent agreement with the analytical solution when $\beta = 0$ [Hicks, 2008].

## References

Balmforth, N. J., A. S. Burbidge, R. V. Craster, J. Salzig, and A. Shen (2000), Visco-plastic models of isothermal lava domes, *J. Fluid Mech.*, 403, 37–65, doi:10.1017/S0022112002001660.

Balmforth, N. J., R. V. Craster, and R. Sassi (2004), Dynamics of cooling viscoplastic domes, *J. Fluid Mech.*, 499, 149–182, doi:10.1017/S0022112003006840.

Barclay, J., M. J. Rutherford, M. R. Carroll, M. D. Murphy, J. D. Devine, J. Gardner, and R. S. J. Sparks (1998), Experimental phase equilibria constraints on preeruptive storage conditions of the Soufrière Hills magma, *Geophys. Res. Lett.*, 25(18), 3437–3440.

Barclay, J., J. E. Johnstone, and A. J. Matthews (2006), Meteorological monitoring of an active volcano: Implications for eruptive prediction, *J. Volcanol. Geotherm. Res.*, 150, 339–358, doi:10.1016/j.jvolgeores.2005.07.020.

Bourgouin, L., H. B. Mühlhaus, A. J. Hale, and A. Arsac (2007), Studying the influence of a solid shell on lava dome growth and evolution using the level set method, *Geophys. J. Int.*, 170, 1431–1438, doi:10.1111/j.1365-246X.2007.03471.x.

Calder, E. S., R. Luckett, R. S. J. Sparks, and B. Voight (2002), Mechanisms of lava dome instability and generation of rockfalls and pyroclastic flows at Soufrière Hills Volcano, Montserrat, in *The Eruption of Soufrière Hills Volcano, Montserrat, From 1995 to 1999*, edited by T. Druitt and B. Kokelaar, *Geol. Soc. Mem.*, 21, pp. 173–190, Geol. Soc., London.

Carn, S. A., R. B. Watts, G. Thompson, and G. E. Norton (2004), Anatomy of a lava dome collapse: The 20 March 2000 event at Soufrière Hills Volcano, Montserrat, *J. Volcanol. Geotherm. Res.*, 131(3–4), 241–264, doi:10.1016/So377-0273(03)00364-0.

Costa, A. (2006), Permeability-porosity relationship: A reexamination of the Kozeny-Carman equation based on a fractal pore-space geometry assumption, *Geophys. Res. Lett.*, 33, L02318, doi:10.1029/2005GL025134.

Couch, S., R. S. J. Sparks, and M. R. Carroll (2001), Mineral disequilibrium in lavas explained by convective self-mixing in open magma chambers, *Nature*, 411, 1037–1039, doi:10.1038/35082540.

Dragoni, M., I. Borsari, and A. Tallarico (2005), A model for the shape of the lava flow front, *J. Geophys. Res.*, 110, B09203, doi:10.1029/2004JB003523.

Dzurisin, D., R. P. Denlinger, and J. G. Rosenbaum (1990), Cooling rate and thermal structure determined from progressive magnetization of the dacite dome at Mount St. Helens, Washington, *J. Geophys. Res.*, 95(B3), 2763–2780.

Edmonds, M., D. Pyle, and C. Oppenheimer (2001), A model for degassing at the Soufrère Hills Volcano, Montserrat, West Indies, based on geochemical data, *Earth Planet. Sci. Lett.*, 186, 159–173, doi:10.1016/S0012-821X(01)00242-4.

Edmonds, M., R. A. Herd, B. Galle, and C. M. Oppenheimer (2003a), Automated, high time-resolution measurements of SO₂ flux at Soufrière Hills Volcano, Montserrat, *Bull. Volcanol.*, 65(8), 578–586, doi:10.1007/s00445-003-0286-x.

Edmonds, M., C. Oppenheimer, D. M. Pyle, R. A. Herd, and G. Thompson (2003b), SO₂ emissions from Soufrière Hills Volcano and their relationship to conduit permeability, hydrothermal interaction and degassing regime, *J. Volcanol. Geotherm. Res.*, 124(1–2), 23–43, doi:10.1016/S0377-0273(03)00041-6.

Elsworth, D., B. Voight, G. Thompson, and S. R. Young (2004), Thermal-hydrologic mechanism for rainfall-triggered collapse of lava domes, *Geology*, 32(11), 969–972.

Fink, J. H., and S. W. Kieffer (1993), Estimates of pyroclastic flow velocities from explosive decompression of lava domes, *Nature*, 363, 612–615.

Francis, P., L. Horrocks, and C. Oppenheimer (2000), Monitoring gases from andesite volcanoes, *Philos. Trans. R. Soc. Lond. A*, 358(1770), 1567–1584, doi:10.1098/rsta.2000.0604.

Hale, A. J., and G. Wadge (2003), Numerical modeling of the growth dynamics of a simple silicic lava dome, *Geophys. Res. Lett.*, 30(19), 2003, doi:10.1029/2003GL018182.

Hale, A. J., L. Bourgouin, and H. B. Mühlhaus (2007), Using the level set method to model endogenous lava dome growth, *J. Geophys. Res.*, 112, B03213, doi:10.1029/2006JB004445.

Hammouya, G., P. Allard, P. Jean-Baptiste, F. Parello, M. P. Semet, and S. R. Young (1998), Pre- and syn-eruptive geochemistry of volcanic gases from Soufriere Hills of Montserrat, West Indies, *Geophys. Res. Lett.*, 25(19), 3685–3688.

Herd, R. A., M. Edmonds, and V. A. Bass (2005), Catastrophic lava dome failure at Soufrière Hills Volcano, Montserrat, 12-13 July 2003, *J. Volcanol. Geotherm. Res.*, 148, 234–252, doi:10.1016/j.jvolgeores.2005.05.003.

Hicks, P. (2008), A thermodynamic model of rainwater and magmatic vapour flow in a porous medium: Triggering of a volcanic lava dome collapse, Ph.D. thesis, Univ. of East Anglia, School of Mathematics, U. K.

Hinch, E. J. (1991), *Perturbation Methods*, Cambridge Univ. Press, Cambridge, U. K.

Iverson, R. M. (1990), Lava domes modeled as brittle shells that enclose pressurized magma, with application to Mount St. Helens, in *IAVCEI Proceedings in Volcanology: Lava Flows and Domes: Emplacement Mechanisms and Hazard Implications*, vol. 2, edited by J. H. Fink, pp. 47–69, Springer, New York.

Mastin, L. G. (1994), Explosive tephra emissions at Mount St. Helens, 1989–1991—the violent escape of magmatic gas following storms?, *Geol. Soc. Am. Bull.*, *106*, 175–185.

Matthews, A. J., and J. Barclay (2004), A thermodynamical model for rainfall-triggered volcanic dome collapse, *Geophys. Res. Lett.*, *31*(5), L05614, doi:10.1029/2003GL019310.

Matthews, A. J., J. Barclay, S. A. Carn, G. Thompson, J. Alexander, R. A. Herd, and C. Williams (2002), Rainfall-induced volcanic activity on Montserrat, *Geophys. Res. Lett.*, *29*(13), 1644, doi:10.1029/2002GL014863.

McNutt, S. R. (1999), Eruptions of Pavlof Volcano, Alaska, and their possible modulation by ocean load and tectonic stresses: Re-evaluation of the hypothesis based on new data from 1984–1998, *Pure Appl. Geophys.*, *155*(2–4), 701–712, doi:10.1007/s000240050284.

McNutt, S. R., and R. J. Beavan (1987), Eruptions of Pavlof Volcano and their possible modulations by ocean load and tectonic stresses, *J. Geophys. Res.*, *92*(B11), 11,509–11,523.

Melnik, O., and R. S. J. Sparks (1999), Nonlinear dynamics of lava dome extrusion, *Nature*, *402*, 37–41, doi:10.1038/46950.

Melnik, O., and R. S. J. Sparks (2002), Dynamics of magma ascent and lava extrusion at Soufrière Hills Volcano, Montserrat, in *The Eruption of Soufrière Hills Volcano, Montserrat, From 1995 to 1999*, edited by T. Druitt and B. Kokelaar, *Geol. Soc. Mem.*, *21*, Geol. Soc., London.

Nakada, S., Y. Miyake, H. Sato, O. Oshima, and A. Fujinawa (1995), Endogenous growth of dacite dome at Unzen volcano (Japan), 1993–1994, *Geology*, *23*(2), 157–160, doi:10.1130/0091-7613(1995)023<0157:EGODDA>2.3.CO;2.

Neri, A. (1998), A local heat transfer analysis of lava cooling in the atmosphere: Application to thermal diffusion-dominated lava flows, *J. Volcanol. Geotherm. Res.*, *81*(3–4), 215–243, doi:10.1016/S0377-0273(98)00010-9.

Neuberg, J. (2000), External modulation of volcanic activity, *Geophys. J. Int.*, *142*(1), 232–240, doi:10.1046/j.1365-246x.2000.00161.x.

Oppenheimer, C., P. W. Francis, D. A. Rothery, R. W. T. Carlton, and L. S. Glaze (1993), Infrared image analysis of volcanic thermal features: Láscar Volcano, Chile, 1984–1992, *J. Geophys. Res.*, *98*(B3), 4269–4286.

Sato, H., T. Fujii, and S. Nakada (1992), Crumbling dacite dome lava and generation of pyroclastic flows at Unzen Volcano, *Nature*, *360*, 664–666, doi:10.1038/360664a0.

Sigurdsson, H. (Ed.) (2000), *Encyclopedia of Volcanoes*, Acad. Press, San Diego, Calif.

Simmons, J., D. Elsworth, and B. Voight (2004), Instability of exogenous lava lobes during intense rainfall, *Bull. Volcanol.*, *66*(8), doi:10.1007/s00445-004-0353-y.

Sparks, R. S. J. (1997), Causes and consequences of pressurisation in lava dome eruptions, *Earth Planet. Sci. Lett.*, *150*(1), 177–189.

Sparks, R. S. J., M. D. Murphy, A. M. Lejeune, R. B. Watts, J. Barclay, and S. R. Young (2000), Control on the emplacement of the andesite lava dome of the Soufrière Hills Volcano, Montserrat by degassing-induced crystallization, *Terra Nova*, *12*(1), 14–20, doi:10.1046/j.1365-3121.2000.00267.x.

Spera, F. (2000), Physical properties of magma, in *Encyclopaedia of Volcanoes*, edited by H. Sigurdsson, pp. 171–190, Academic, San Diego, Calif.

Taron, J., D. Elsworth, G. Thompson, and B. Voight (2007), Mechanisms for rainfall-concurrent lava dome collapses at Soufrière Hills Volcano, 2000–2002, *J. Volcanol. Geotherm. Res.*, *160*, 195–209, doi:10.1016/j.jvolgeores.2006.10.003.

Urai, M. (2000), Volcano monitoring with Landsat TM shortwave infrared bands: The 1990–1994 eruption of Unzen Volcano, Japan, *Int. J. Remote Sens.*, *21*(5), 861–872, doi:10.1080/014311600210335.

Vaughan, R. G., S. J. Hook, M. S. Ramsey, V. J. Realmuto, and D. J. Schneider (2005), Monitoring eruptive activity at Mount St. helens with TIR image data, *Geophys. Res. Lett.*, *32*, L19305, doi:10.1029/2005GL024112.

Watts, R. B., R. A. Herd, R. S. J. Sparks, and S. R. Young (2002), Growth patterns and emplacement of the andesitic lava dome at Soufrière Hills Volcano, Montserrat, in *The Eruption of Soufrière Hills Volcano, Montserrat, From 1995 to 1999*, edited by T. Druitt and B. Kokelaar, *Geol. Soc. Mem.*, *21*, pp. 115–152, Geol. Soc., London.

Woods, A. W., R. S. J. Sparks, L. J. Ritchie, J. Batey, C. Gladstone, and M. I. Bursik (2002), The explosive decompression of a pressurized volcanic dome: The 26 December 1997 collapse and explosion of Soufrière Hills Volcano, Montserrat, in *The Eruption of Soufrière Hills Volcano, Montserrat, From 1995 to 1999*, edited by T. Druitt and B. Kokelaar, *Geol. Soc. Mem.*, *21*, pp. 457–465, Geol. Soc., London.

Yamasato, H., S. Kitagawa, and M. Komiya (1998), Effect of rainfall on dacitic lava dome collapse at Unzen Volcano, Japan, *Pap. Meteorol. Geophys.*, *48*(3), 73–78, doi:10.2467/mripapers.48.73.

———————————

M. J. Cooker and P. D. Hicks, School of Mathematics, University of East Anglia, Norwich, NR4 7TJ, UK. (m.cooker@uea.ac.uk; p.hicks@uea.ac.uk)

A. J. Matthews, School of Environmental Sciences, University of East Anglia, Norwich, NR4 7TJ, UK. (a.j.matthews@uea.ac.uk)